

NJC

Accepted Manuscript



This is an *Accepted Manuscript*, which has been through the Royal Society of Chemistry peer review process and has been accepted for publication.

Accepted Manuscripts are published online shortly after acceptance, before technical editing, formatting and proof reading. Using this free service, authors can make their results available to the community, in citable form, before we publish the edited article. We will replace this *Accepted Manuscript* with the edited and formatted *Advance Article* as soon as it is available.

You can find more information about *Accepted Manuscripts* in the [Information for Authors](#).

Please note that technical editing may introduce minor changes to the text and/or graphics, which may alter content. The journal's standard [Terms & Conditions](#) and the [Ethical guidelines](#) still apply. In no event shall the Royal Society of Chemistry be held responsible for any errors or omissions in this *Accepted Manuscript* or any consequences arising from the use of any information it contains.

The solvothermal synthesis and enhanced photocatalytic activity of Zn²⁺ doped BiOBr hierarchical nanostructures

Xu Chun Song^{a*}, Yi Fan Zheng^b, Hao Yong Yin^c, Jia Ning Liu^a, Xue Dan Ruan^a

^aDepartment of Chemistry, Fujian Normal University, Fuzhou 350007, P. R. China

^bResearch Center of Analysis and Measurement, Zhejiang University of Technology, Hangzhou 310014, P. R. China

^cInstitute of Environmental Science and Engineering, Hangzhou Dianzi University, Hangzhou, 310018, P. R. China

Abstract: Novel visible-light-induced Zn-doped BiOBr hierarchical nanostructures were successfully prepared by solvothermal methods. The photocatalytic activity of the as-synthesized samples was evaluated using RhB as target pollutant. The Zn-doped BiOBr hierarchical nanostructures exhibited significantly enhanced visible light-induced photocatalytic efficiency for the degradation of RhB compared with pure BiOBr. The Zn-doped BiOBr with $R_{Zn}=0.1$ (R_{Zn} defined as the atomic ratio of Zn to Bi) showed the highest photocatalytic activity with decolorization efficiency almost 100% after 15 min. The enhanced photocatalytic ability could be attributed to the efficient separation of photogenerated electron-hole pairs. Moreover, the role of the active species is also evaluated by adding different scavengers during the photodegradation of RhB. A possible mechanism of the enhancement of visible light performance on Zn-doped BiOBr photocatalysts was also proposed on basis of the experimental results.

Keywords: A. nanostructures, B. solvothermal, C. electron microscopy, D. catalytic properties

1. Introduction

Effluents containing large amounts of dyes are important sources of water pollution, because colored dye in wastewater can threaten the aquatic life and endanger human health. Therefore, people have been taking action to treat dye wastewaters [1]. Heterogeneous photocatalysis have aroused extensive interest due to their applications in decomposing organic dye for environmental

*Corresponding author. Tel: +86-591-87441126; fax: +86-591-83465376

E-mail: songxuchunfj@163.com (X.C. Song).

remediation [2]. Among the diverse photocatalysts, TiO_2 is the famous one due to its high activity, low price, nontoxic and long-term stability [3, 4]. However, it can only be activated by the ultraviolet light, which comprises less than 5% of the solar spectrum [5]. Considering visible light accounts for 43% energy in solar spectrum, intensive efforts have been made to develop efficient visible-light-driven photocatalysts, such as inorganic bismuth compounds (BiVO_4 [6], Bi_2WO_6 [7,8], Bi_2MoO_6 [9], BiFeO_3 [10], BiOX ($X=\text{Cl, Br, I}$)[11], BiFeO_3 [12]).

Bismuth oxyhalides (BiOBr) are V–VI–VII ternary compounds with tetragonal matlockite structure. Over the past few years, they have been investigated because of their unique visible light photocatalytic performance in degradation of organic contaminants. Various BiOBr structures such as microspheres [13], nanobelts [14], microflowers [15], nanoplates [16] have been prepared, and these BiOBr with various morphologies and dimensionalities present high photocatalytic activity. However, the photocatalytic activity of BiOBr is still cannot meet the requirements of practical application and it is necessary to find new approaches to improve their photocatalytic efficiency. Therefore, numerous techniques have been adopted to enhance their photocatalytic efficiency, such as ion doping [17] and coupling with other semiconductors [18]. Many BiOBr composite photocatalysts ($\text{BiOBr-g-C}_3\text{N}_4$ [19], Cd-BiOBr [20], BiOBr-Graphene [21], BiOI-BiOBr [22], BiOCl-BiOBr [23], AgBr-BiOBr [24], $\text{BiOBr-ZnFe}_2\text{O}_4$ [25], BiOBr-TiO_2 [26] and $\text{BiOCl/Bi}_2\text{MoO}_6$ [27]) were prepared and all of which showed enhanced photocatalytic efficiencies. However, there are few reports on investigating the doping of nonmetal elements and transition metal elements in BiOBr . Moreover, the transition metal elements have many valences and the trace transition metal ions doped in the BiOBr matrix may be potential trap of photogenerated electron–hole pairs, then prolong the lifetime of electrons and holes and consequently increase the photocatalytic activity. Recently, a novel and efficient visible-light-induced BiOBr photocatalyst with Ti doping and Ag decorating was successfully obtained [28]. The Ti-doped BiOBr photocatalysts displayed higher activity for the degradation of RhB under visible light irradiation [29]. Fe-doped BiOBr hollow microspheres also exhibited excellent photocatalytic activity [30]. However, to the best of our knowledge, there are no studies on synthesis and photocatalytic performance of Zn-doped BiOBr photocatalyst.

In this paper, visible light-activated Zn-doped BiOBr hierarchical nanostructures were successfully synthesized by a facile and rapid solvothermal method. The photocatalytic efficiency

of the Zn-doped BiOBr was evaluated by decolorizing RhB under visible light irradiation. Moreover, the effect of Zinc doping on the structure and photocatalytic activity of BiOBr catalyst was also studied in detail. The photocatalytic activity of Zn-doped BiOBr was greatly enhanced as compared to pure BiOBr. The enhancement of photocatalytic activity on the Zn-doped BiOBr may be related to the doped Zn which could act as holes traps and consequently suppress the recombination of electrons and holes.

2. Experimental section

2.1 Synthesis of Zn-doped BiOBr hierarchical nanostructures

All the chemicals were of analytical purity and used without further purification. In the typical preparation, 5mmol of $\text{Zn}(\text{NO}_3)_2 \cdot 6\text{H}_2\text{O}$ and $\text{Bi}(\text{NO}_3)_3 \cdot 5\text{H}_2\text{O}$ with a Zn/Bi molar ratio of 0, 0.02, 0.06, 0.10 and 0.14 were dissolved in 20 mL ethylene glycol under magnetically stirring. 5mmol of KBr were dissolved in 20 mL ethylene glycol, and then the resultant solution was added slowly to the above $\text{Bi}(\text{NO}_3)_3$ solution with vigorous stirring. Next, the suspension was transferred into a 50mL teflon-lined stainless steel, followed by a solvothermal treatment at 160 °C for 12 h. After cooling to room temperature naturally, the obtained precipitates were separated centrifugally and washed with deionized water and ethanol for several times, and the samples were dried at 60 °C for 5 h. For convenience of description, the value of R_{Zn} is used to describe the atomic ratio of Zn to Bi and represents 0, 0.02, 0.06, 0.10 and 0.14 atomic ratios.

2.2 Characterization

The phase structures of the obtained samples were analyzed with a Thermo ARL SCINTAG X'TRA diffractometer using Cu K α radiation ($\lambda = 0.154056$ nm), and recorded with 2θ ranging from 20–80°. The morphologies of the samples were investigated by a Hitachi S-4700 field emission scanning electron microscope (SEM, scanning voltages 15 kV) equipped with Energy-dispersive X-ray detector (EDS, Thermo Noran VANTAG-ESI) and Tecnai G2 F30 transmission electron microscopy (TEM, accelerating voltage 200 kV). UV–vis diffuse reflectance spectra of the as-prepared products were analyzed on an UV-vis spectrophotometer (Lambda 850) using BaSO_4 as the reference. The Brunauer–Emmett–Teller (BET) specific surface area was measured using a Micrometrics ASAP 2000 surface area analyzer. The photocurrents were measured using an electrochemical workstation (CHI-660C, China) with a standard three-electrode system, which employed ITO glass coated with the as-prepared samples (0.1 mg)

as the working electrode, a Pt wire as the counter electrode, and a saturated Ag/AgCl electrode as a reference electrode. A 300 W xenon lamp was utilized as light source. A 0.1 M Na₂SO₄ aqueous solution was used as electrolyte.

2.3 Photocatalytic experiments

Photocatalytic activities of the Zn-doped BiOBr were evaluated by the photodegradation of Rhodamine B (RhB) in aqueous solution. The photocatalytic experiments were carried out under visible light irradiation with a 300W Xe lamp as light source and a 420 nm cutoff filter equipped to provide visible light. In every experiment, 0.1 g of the as-prepared photocatalyst was suspended in 200 mL RhB aqueous solution ($C_0=2\times 10^{-5}$ mol/L) with constant stirring. Prior to irradiation, the suspensions were stirred for 1 h in dark to ensure the establishment of adsorption–desorption equilibrium between the catalyst and RhB. Subsequently, photocatalytic test was conducted with 5 mL reacting solution sampled and then centrifuged to remove the photocatalysts at every irradiation time intervals. The change of RhB concentrations (C) was monitored by measuring the maximum absorbance at 553 nm for RhB using a UV759S UV-Vis spectrophotometer.

3. Results and discussion

3.1 Morphology and microstructure

The microstructures, morphologies and particle sizes of pure BiOBr and Zn-doped BiOBr with different zinc contents were investigated by SEM and TEM. It can be seen from Figure 1a that pure BiOBr is comprised of many microspheres with the range from 2 to 10 μm in diameters. The SEM images of Zn-doped BiOBr with different zinc contents are shown in Figure 1b–e. It can be found that the morphologies of the Zn-doped BiOBr are similar with pure BiOBr. However, with the increase of Zn amount, it could be observed that much more Zn-doped BiOBr microspheres with an size ranging from 1 to 2 μm were obtained, indicating that the Zn-doping can partly reduce the particle size of the BiOBr microspheres which may act as the inhibitor for crystal growth in BiOBr preparation. Figure 1f shows the high magnification SEM image of Zn-doped BiOBr microspheres with $R_{\text{Zn}}=0.1$. Careful observation reveals that Zn-doped BiOBr microspheres are formed of many nanosheets stacked together. Therefore, the TEM image further confirms that as-prepared Zn-doped BiOBr microsphere is consisted of self-assembled nanosheets (Figure 1g). EDS experiment was used to further identify the element composition of Zn-doped BiOBr hierarchical nanostructures with $R_{\text{Zn}}=0.1$ and the results are shown in Figure 1h. The

obvious signals for Br, Bi and O elements were observed in the spectra together with a weak signal of zinc element.

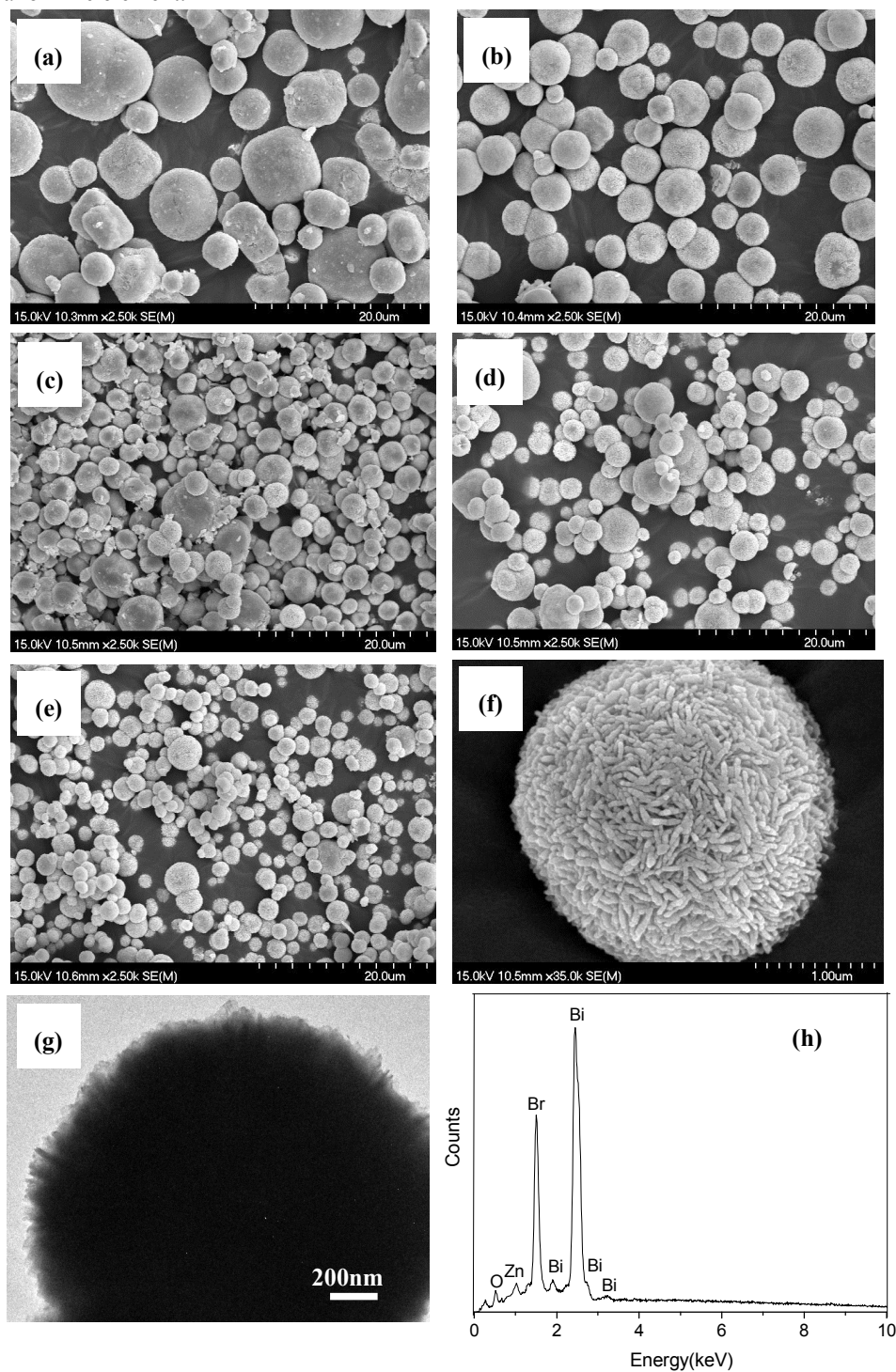


Figure 1. SEM images of the Zn-doped BiOBr samples with different R_{Zn} values: (a) 0, (b) 0.02, (c) 0.06, (d) 0.10, (e) 0.14, respectively. (f) A magnified SEM and (g) TEM of single Zn-doped BiOBr samples with $R_{Zn}=0.10$. (h) EDS of Zn-doped BiOBr with $R_{Zn}=0.10$.

3.2 XRD analysis

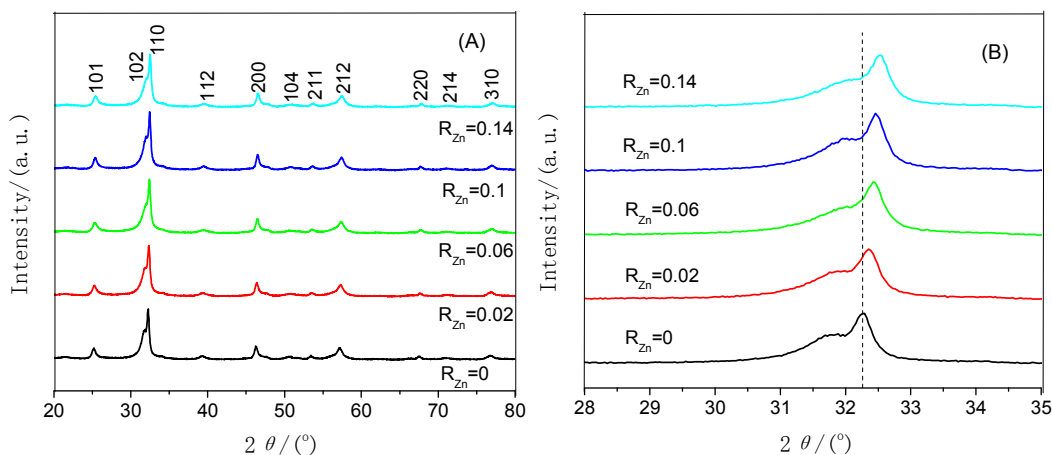


Figure 2. (A) XRD diffraction patterns of the Zn-doped BiOBr samples with different R_{Zn} values. (B)

Diffraction peak positions of the (110) plane in the range of $2\theta = 28\text{-}35^\circ$.

Table 1. The cell parameters of BiOBr doped with different contents of zinc ions.

Zn-doping concentrations	the cell parameters		
	a	b	c
0	3.924Å	3.924Å	8.107Å
0.02	3.917Å	3.917Å	8.107Å
0.06	3.913Å	3.913Å	8.105Å
0.10	3.910Å	3.910Å	8.104Å
0.14	3.903Å	3.903Å	8.103Å

Fig.2A shows the XRD patterns of the pure BiOBr and Zn-doped BiOBr with different zinc contents. It could be seen that all of the diffraction peaks of the as-prepared samples match well with the standard data of the tetragonal phase of BiOBr (JCPDS card no. 78-0348). No signal of any other diffraction peaks was observed for all samples, which indicated that the introducing of Zn-ions did not significantly change the crystal structure of BiOBr. Further observation of the (110) diffraction peaks in the range of $28\text{-}35^\circ$ is shown in Fig.2B. The peak position of zinc doped BiOBr shifts slightly towards a higher 2θ value with an increase of the zinc concentrations. The

other diffraction peaks show the similar results. It is known that the differences between the ionic radius can induce changes in the lattice parameters [31]. The cell parameters of Zn-doped BiOBr with different zinc contents are shown on Table 1. Because ionic radius of 0.074 nm for Zn^{2+} is smaller than that of 0.103 nm for the Bi^{3+} , and the doped Zn^{2+} may be incorporated into the BiOBr matrix by substituting for Bi^{3+} lattice sites, the lattice parameters decrease with the increase of the Zn^{2+} concentration, and accordingly the observed diffraction peak shift toward a higher angle.

3.3 UV-vis DRS analysis

The UV-vis diffuse reflectance spectroscopy (DRS) of pure BiOBr and Zn-doped BiOBr are shown in Fig. 3A. It can be seen that the pure BiOBr has an absorption edge at about 425 nm. However, the absorption edge of Zn-doped BiOBr has a little shift to a longer wavelength with the increase of zinc contents, suggesting that the absorption of visible light may be caused by the transition of impurity energy levels [32]. The band gap (E_g) of the pure BiOBr and Zn-doped BiOBr can be calculated by a classical formula [33]:

$$A(h\nu - E_g)^{n/2} = ah\nu \quad (1)$$

where A , h , ν , a and E_g are a constant, Planck constant, light frequency, absorption coefficient, and band gap energy, respectively. Among them, n depends on the type of optical transition of a semiconductor ($n = 1$ for direct transition and $n = 4$ for indirect transition). For BiOBr, the value of n is 4 [34]. The band gaps of the pure BiOBr and Zn-doped BiOBr with $R_{\text{Zn}}=0.1$ were calculated to be 2.68 and 2.51 eV, respectively (Fig. 3B).

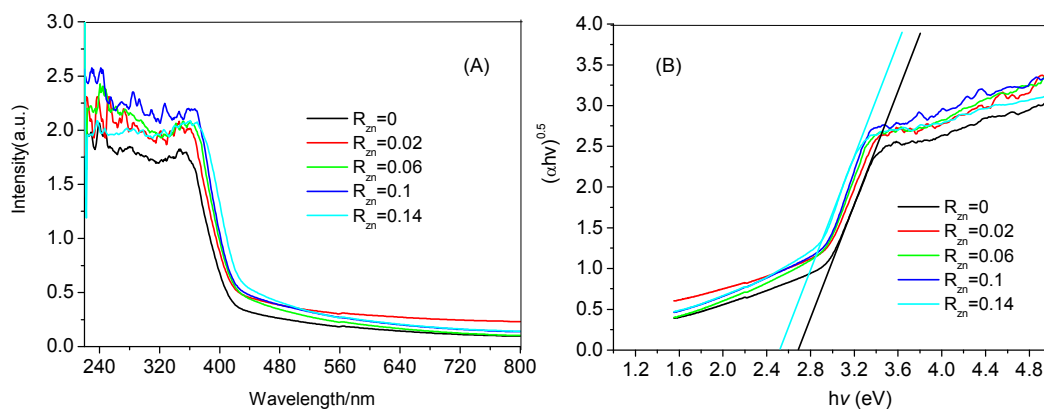


Figure 3. (A) UV-vis diffuse reflectance spectra of the Zn-doped BiOBr samples with different R_{Zn} values, (B) plots of the $(\alpha h\nu)^{1/2}$ versus $h\nu$ of Zn-doped BiOBr samples.

3.4 Photocatalytic activity

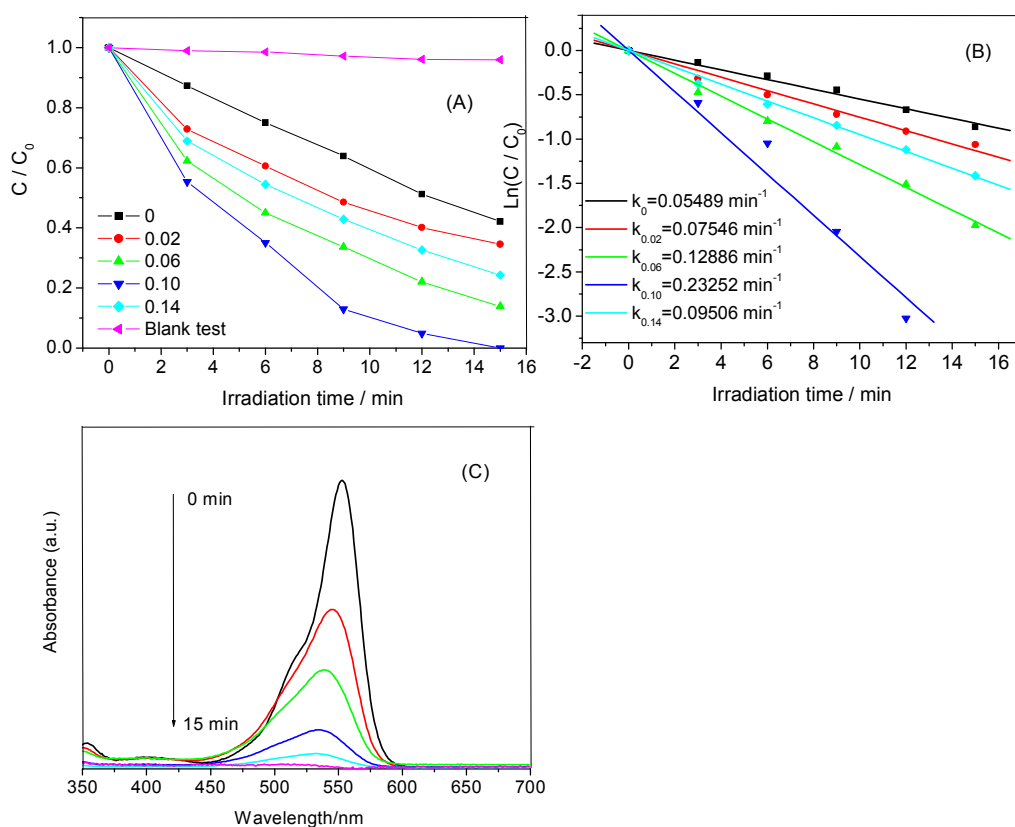


Figure 4. (A) the photocatalytic activity of the Zn-doped BiOBr samples, (B) UV-vis spectral changes of the degradation of RhB dye by the Zn-doped BiOBr samples with $R_{Zn}=0.10$ catalyst.

To study the photocatalytic activities of the samples, we investigated the photocatalytic degradation of RhB under visible light irradiation. Fig. 4A shows the decolorization efficiencies of RhB molecules by different photocatalysts, where C_0 is the initial concentration after the adsorption equilibrium on the photocatalyst before irradiation and C is the concentration of RhB during the irradiation time. The blank test (without any photocatalysts) shows extremely low photodegradation ability on RhB, which could be almost ignored. Only about 57% of the RhB is decolorized by pure BiOBr after irradiation for 15 min. Comparing with the pure BiOBr, all the Zn-doped BiOBr exhibit higher photocatalytic efficiency, which indicated that zinc doping could effectively improve the photocatalytic performance of BiOBr. It can be found that the Zn-doped BiOBr with $R_{Zn}=0.1$ shows the highest photocatalytic activity with the decolorization efficiency arriving to nearly 100% after 15 min irradiation. The photocatalysis kinetics of the RhB

degradation were found to fit a pseudo-first order model: $\ln(C/C_0) = k$, where k is the kinetic constant. The pseudo-first-order rate constants are calculated in Fig. 4B. As can be observed from the Zn-doped BiOBr microspheres the photocatalytic activities could be evidently enhanced with the increase of Zn^{2+} content at Zn-doping concentration lower than 0.10. However, when the Zn^{2+} concentration increased continually to $R_{Zn}=0.14$, the photocatalytic activities of Zn-doped BiOBr decreased obviously. This result suggested that photocatalytic ability of the samples was strongly dependent on the Zn-doping amount. Fig. 4C shows the time-dependent absorption spectra of RhB solution photocatalyzed by the Zn-doped BiOBr with $R_{Zn}=0.1$. It can be seen obviously that the color of the RhB solution changed from initially pink to colorless after irradiation for 15 min. The maximum absorption of RhB solution shifts from 553 to 532 nm. The shift can be attributed to the RhB photodegradation occurred via two competitive processes: N-demethylation and the destruction of the conjugated structure [35].

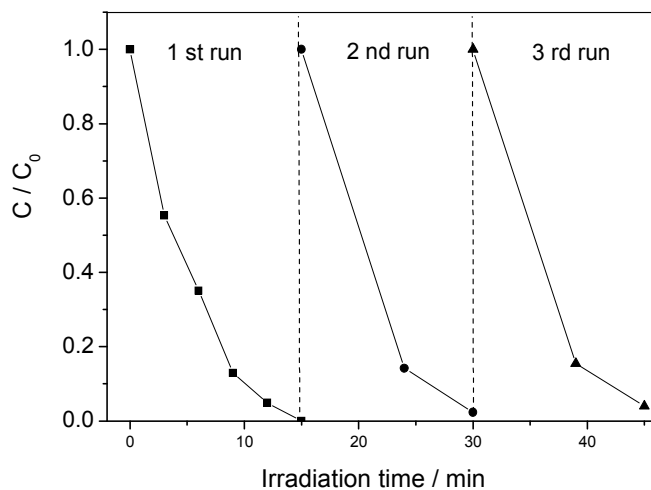


Figure 5. Repetitive test of the Zn-doped BiOBr samples with $R_{Zn}=0.10$ catalyst.

Besides the higher activity, the recyclability of the photocatalyst is also very important factors for its practical application. Therefore, the recycling degradation tests were applied to evaluate the stability of the Zn-doped BiOBr with $R_{Zn}=0.1$ (Fig. 5). After three recycles, the Zn-doped BiOBr catalyst had a little loss of efficiency due to the loss of catalyst during washing and recycling process, but still exhibited good photocatalytic activity. The TEM and XRD of Zn-doped BiOBr after photodegradation of RhB shows no changes in the morphologies and tetragonal phase of photocatalyst, indicating the catalyst possesses excellent stability and reusability.

3.5 Discussion of degradation mechanism

Photocatalytic performance was governed by some crucial factors, such as BET surface area, and separation efficiency of photogenerated electrons and holes. A large surface area is helpful to provide more photocatalytic reaction sites, which are favorable to the photocatalytic efficiency [36]. It can be seen from Table 2 that Zn-doped BiOBr have higher surface area than that of pure BiOBr, the specific surface area increases with the increase of the zinc content. However, the specific surface area of Zn-doped BiOBr with $R_{Zn}=0.10$ and 0.14 were not consistent with the photocatalytic activity. This result indicates that the specific surface area is not the decisive factor in association with the photocatalytic activity of Zn-doped BiOBr.

Table 2. Specific surface area of BiOBr doped with different contents of zinc ions.

Zn-doping concentrations	0	0.02	0.06	0.10	0.14
Surface area ($\text{m}^2 \text{g}^{-1}$)	11.43	13.16	15.84	16.73	16.82

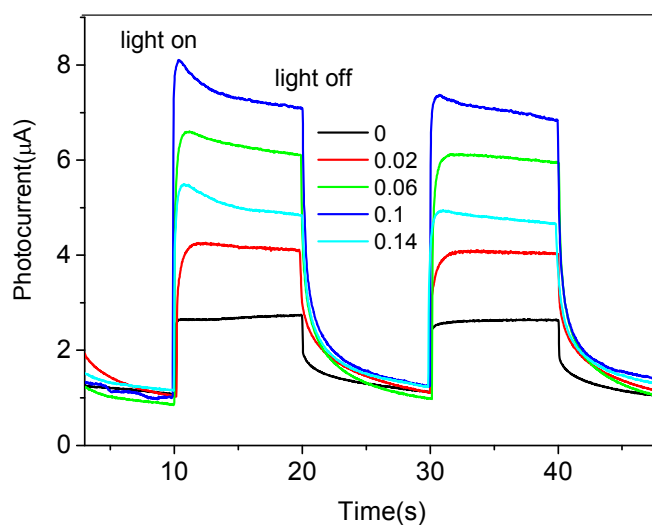


Figure 6. Photocurrent response for the Zn-doped BiOBr samples with different R_{Zn} values.

As we all known, the photocurrent is widely regarded as the efficient evidence demonstrating the separation of photo-generated carriers in the photocatalysts. Fig. 6 shows the transient photocurrent responses for a series of Zn-doped BiOBr during repeating light on/off cycles under visible light irradiation. It is clear to see that all of the photocurrent generated from the Zn-doped

BiOBr were larger than that of pure BiOBr which may indicate more efficiency of the photogenerated electrons and holes separation after Zn doping. These Zn^{2+} may be positioned into the BiOBr crystal lattice by substituting of Bi^{3+} lattice sites. As is known, upon light irradiation, electrons can be excited from the valence band to the conduction band, leaving the corresponding holes in the valence band. In this case, Zn d^{10} might be deeper than VB state of BiOBr. Therefore, the suitable amount of Zn^{2+} dopants may capture photogenerated holes and decrease the rate of recombination of electron-hole and accelerate photocatalytic reaction. However, the charge capture centers maybe become the recombination centers by overloading dopants [37]. Therefore, with a further increase of Zn concentration to 0.14, the photogenerated current density decreases due to fact that high concentrations of Zn may also act as a recombination center.

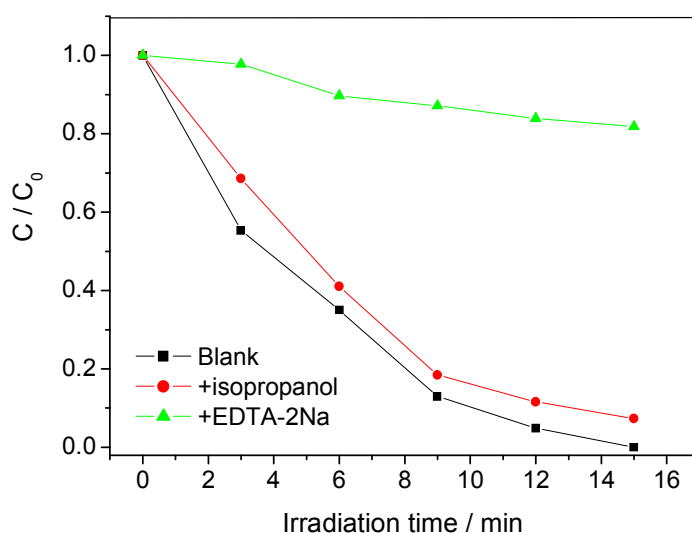


Figure 7. The effects of EDTA-2Na and isopropanol on the decolorization of RhB with the Zn-doped BiOBr samples with $R_{Zn}=0.10$ catalyst.

The reactive species may be different during photocatalytic reaction on different photocatalysts. To clarify the photodegradation mechanism, isopropyl alcohol and EDTA-2Na were adopted as $\cdot OH$ and hole scavenger respectively. Fig. 7 illustrates the photodecolorization of RhB over Zn-doped BiOBr with $R_{Zn}=0.10$ in different conditions. The decolorization efficiency of RhB decreases from 100% to 92% and from 100% to 19% with the addition of isopropyl alcohol and EDTA-2Na, respectively. This indicates that the holes play important role in this reaction.

4. Conclusion

In summary, the Zn doped BiOBr hierarchical nanostructures as novel visible-light-induced photocatalysts were successfully synthesized by a simple solvothermal method. The photocatalytic performance of the Zn doped BiOBr samples is highly dependent on Zn content. With the increase of the Zn²⁺ addition, the photocurrent and surface area of the photocatalysts were greatly increased, which greatly improved the photocatalytic activity of the BiOBr microspheres. The enhanced photocatalytic activity can be attributed to the high separation efficiency of the photogenerated electron-hole pairs and the increases of the BET surface area of the photocatalysts. The main active species and their roles in the Zn doped BiOBr photocatalysis were investigated which suggested that the holes played important role in this photocatalytic reaction.

Acknowledgment

This work is financially supported by the National Nature Science Foundation of China (No. 21273034) and the support of Training Programs of Innovation and Entrepreneurship for Undergraduates of Fujian Normal University (No. cxxl-2015100).

Reference

- [1] Z. Yu, B. Detlef, D. Ralf, L. Song and L. Lu, *J. Mol. Catal. A: Chem.*, 2012, 365, 1–7.
- [2] Z. Jiang, F. Yang, G. Yang, L. Kong, M. O. Jones, T. Xiao and P. P. Edwards, *J. Photoch. Photobio. A: Chem.*, 2010, 212, 8–13.
- [3] A. Maurizio, A. Vincenzo and D. P. Agatino, *J. Phys. Chem. B*, 2004, 108, 3303–3310.
- [4] M. K. Nowotny, L. R. Sheppard and T. Bak, *J. Phys. Chem. C*, 2008, 112, 5275–5300.
- [5] S. U. M. Khan, M. Al-Shahry and W. B. Ingler, *Science*, 2002, 297, 2243–2245.
- [6] Z. Y. Bian, Y. Q. i Zhu, J. X. Zhang, A. Z. Ding and H. Wang, *Chemosphere*, 2014, 117, 527–531.
- [7] X. C. Song, Y. F. Zheng, R. Ma, Y. Y. Zhang and H. Y. Yin, *J. Hazar. Mater.*, 2011, 192, 186–191.
- [8] A. Singh, D. P. Dutta, M. Roy, A. K. Tyagi and M. H. Fulekar, *J. Mater. Sci.*, 2014, 49, 2085–2097.
- [9] F. Duan, Y. Zheng and M. Chen, *Mater. Lett.*, 2011, 65, 191–193.
- [10] X. Lv, J. Xie, Y. Song and J. Lin, *J. Mater. Sci.*, 2007, 42, 6824–6827.
- [11] L. Chen, R. Huang, M. Xiong, Q. Yuan, J. He and J. Jia, *Inorg. Chem.*, 2013, 52, 11118–11125.
- [12] T. Gao, Z. Chen, Y. Zhu, F. Niu, Q. Huang, L. Qin, X. Sun and Y. Huang, *Mater. Res. Bull.*, 2014, 59, 6–12.
- [13] Y. H. Feng, L. Li, J. W. Li, J. F. Wang and L. Liu, *J. Hazard. Mater.*, 2011, 192, 538–544.
- [14] J. W. Wang and Y. D. Li, *Chem. Commun.*, 2003, 232, 2320–2321.
- [15] Y. J. Chen, M. Wen and Q. S. Wu, *CrystEngComm*, 2011, 13, 3035–3039.
- [16] Z. T. Deng, D. Chen, B. Peng and F. Q. Tang, *Cryst. Growth Des.*, 2008, 8, 2995–3003.
- [17] H. Fu, S. Zhang, T. Xu, Y. Zhu and J. Chen, *Environ. Sci. Technol.*, 2008, 42, 2085–2091.
- [18] Y. Sun, W. Zhang, T. Xiong, Z. Zhao, F. Dong, R. Wang and W. Ho, *J. Colloid Interf. Sci.*, 2014, 418, 317–323.
- [19] L. Ye, J. Liu, Z. Jiang, T. Penga and L. Zan, *Appl. Catal. B: Environ.*, 2013, 142–143, 1–7.
- [20] Z. S. Liu, B. T. Wu, Y. B. Zhu, F. Wang and L. G. Wang, *J. Colloid Interf. Sci.*, 2013, 392, 337–342.
- [21] Z. Ai, W. Ho and S. Lee, *J. Phys. Chem. C*, 2011, 115, 25330–25337.

- [22] J. Cao, B. Xu, H. Lin, B. Luo and S. Chen, *Chem. Eng. J.*, 2012, 185–186, 91–99.
- [23] J. Zhang, J. Xia, S. Yin, H. Li, H. Xu, M. He, L. Huang and Q. Zhang, *Colloid. Surf. A: Physicochem. Eng. Asp.*, 2013, 420, 89–95.
- [24] L. Kong, Z. Jiang, H. H. Lai, R. J. Nicholls, T. Xiao, M. O. Jonesd and P. P. Edwards, *J. Catal.*, 2012, 293, 116–125.
- [25] L. Kong, Z. Jiang, T. Xiao, L. Lu, M. O. Jonesac and P. P. Edwards, *Chem. Commun.*, 2011, 47, 5512–5514.
- [26] X. X. Wei, H. Cui, S. Guo, L. Zhao and W. Li, *J. Hazar. Mater.*, 2013, 263, 650–658.
- [27] Y. Zuo, C. Wang, Y. Sun and J. Cheng, *Mater. lett.*, 2015, 139, 149–152.
- [28] G. Jiang, R. Wang, X. Wang, X. Xi, R. Hu, Y. Zhou, S. Wang, T. Wang and W. Chen, *Appl. Mater. Interfaces*, 2012, 4, 4440–4444.
- [29] R. Wang, G. Jiang, X. Wang, R. Hu, X. Xi, S. Bao, Y. Zhou, T. Tong, S. Wang, T. Wang and W. Chen, *Powder Technol.*, 2012, 228, 258–263.
- [30] G. Jiang, X. Wang, Z. Wei, X. Li, X. Xi, R. Hu, B. Tang, R. Wang, S. Wang, T. Wang and W. Chen, *J. Mater. Chem. A*, 2013, 1, 2406–2410.
- [31] G. Huang and Y. Zhu, *CrystEngComm*, 2012, 14, 8076–8082.
- [32] S. Shen, L. Zhao, X. Guan and L. Guo, *J. Phys. Chem. Solids*, 2012, 73, 79–83.
- [33] W. S. Kuo and P. H. Ho, *Dyes Pigments*, 2006, 71, 212–217.
- [34] S. Shenawi-Khalil, V. Uvarov, S. Fronton, I. Popov and Y. Sasson, *J. Phys. Chem. C*, 2012, 116, 11004–11012.
- [35] D. Zhang, J. Li, Q. Wang and Q. Wu, *J. Mater. Chem. A*, 2013, 1, 8622–8629.
- [36] J. Xia, L. Xu, J. Zhang, S. Yin, H. Li, H. Xu and J. Di, *CrystEngComm*, 2013, 15, 10132–10141.
- [37] A. S. Alshammari, L. Chi, X. Chen, A. Bagabas, D. Kramer, A. Alromaeha and Z. Jiang, *RSC Adv.*, 2015, 5, 27690–27698.

The Zn-doped BiOBr hierarchical nanostructure was fabricated by solvothermal methods. The photocatalytic activity of BiOBr was greatly enhanced by Zn-doping.

